Molecular Psychiatry
https://doi.org/10.1038/s41380-019-0363-y

IMMEDIATE COMMUNICATION

Serotonin-induced hyperactivity in SSRI-resistant major depressive disorder patient-derived neurons

Krishna C. Vadodaria[1] · Yuan Ji[2,3] · Michelle Skime[4] · Apua Paquola[1,5] · Timothy Nelson[3] · Daniel Hall-Flavin[4] · Callie Fredlender[1] · Kelly J. Heard[1] · Yalin Deng[1] · Amy T. Le[1] · Sonia Dave[1] · Lianna Fung[1] · Xinyi Li[1] · Maria C. Marchetto[1] · Richard Weinshilboum[3] · Fred H. Gage[1]

Received: 31 August 2018 / Revised: 2 December 2018 / Accepted: 11 January 2019

Abstract

Selective serotonin reuptake inhibitors (SSRIs) are the most prescribed antidepressants. They regulate serotonergic neurotransmission, but it remains unclear how altered serotonergic neurotransmission may contribute to the SSRI resistance observed in approximately 30% of major depressive disorder (MDD) patients. Patient stratification based on pharmacological responsiveness and the use of patient-derived neurons may make possible the discovery of disease-relevant neural phenotypes. In our study from a large cohort of well-characterized MDD patients, we have generated induced pluripotent stem cells (iPSCs) from SSRI-remitters and SSRI-nonremitters. We studied serotonergic neurotransmission in patient forebrain neurons in vitro and observed that nonremitter patient-derived neurons displayed serotonin-induced hyperactivity downstream of upregulated excitatory serotonergic receptors, in contrast to what is seen in healthy and remitter patient-derived neurons. Our data suggest that postsynaptic forebrain hyperactivity downstream of SSRI treatment may play a role in SSRI resistance in MDD.

Introduction

Psychiatric disorders are a leading cause of morbidity worldwide, and major depressive disorder (MDD) is the most prevalent psychiatric disorder, with an estimated 15 million adults suffering every year in the United States [1–3]. Selective serotonin (5-HT) reuptake inhibitors (SSRIs) are the most widely used antidepressants for managing MDD symptoms and clinical features, but an estimated 30–40% of MDD patients fail to respond to SSRIs. Furthermore, the underlying mechanisms of SSRI resistance and MDD itself are largely unknown [4]. Animal models of depression have provided insights into mechanisms associated with MDD endophenotypes; however, treatment resistance remains difficult to study in these models, and how these findings apply to human mental illness and its treatments remains difficult to assess. Further, it remains difficult to examine treatment resistance in animal models, with limited possibilities for extrapolation to humans. In humans, gene expression and histology can be studied in postmortem tissue, and brain regions can be studied using functional imaging in living people; however, it is difficult to decipher the causes or consequences of MDD with these tools. Large-scale human genome-wide association (GWA) studies have identified sets of disease-associated variants for heritable polygenic disorders like schizophrenia (SCZD) [5], but such an approach has proven to be challenging for MDD [6]. Meta-analyses of multiple GWA studies comparing over 130,000 MDD cases vs. controls found key risk loci and MDD-associated gene sets that overlapped with autism and SCZD risk loci. The genetic markers also

Supplementary information The online version of this article (https://doi.org/10.1038/s41380-019-0363-y) contains supplementary material, which is available to authorized users.

✉ Fred H. Gage
gage@salk.edu

[1] Laboratory of Genetics, The Salk Institute for Biological Studies, 10010 North Torrey Pines Road, La Jolla, CA, USA

[2] University of Utah School of Medicine, Salt Lake City, UT, USA

[3] Department of Molecular Pharmacology and Experimental Therapeutics, Mayo Clinic, Rochester, MN, USA

[4] Department of Psychiatry and Psychology, Mayo Clinic, Rochester, MN, USA

[5] Lieber Institute for Brain Development, 855N Wolfe St, Ste 300, Baltimore, MD, USA

Published online: 30 January 2019

correlated with variables such as lower educational attainment and higher body mass index. These findings suggest that MDD, at least by the current clinical definition, may not be a biologically distinct phenomenon but rather a collection of multiple negative outcomes stemming from a complex interplay between biological and environmental factors [7]. Therefore, it is not surprising that discovering the genes and neural mechanisms associated with MDD has been notoriously difficult due to patient heterogeneity and the limitations of generating rodent models that recapitulate the complex behavioral, cellular, and molecular differences underlying the human pathology.

Stratifying patients based on biological phenotypes, for example, extreme pharmacological responsiveness, offers an approach for examining a subset of patients and identifying treatment- or resistance-associated phenotypes. Induced pluripotent stem cell (iPSC) technology offers a unique opportunity for generating neural cells from subsets of psychiatric patients, enabling the study of cellular and molecular aspects of neurotransmission at a scale previously not possible [8]. Several studies using psychiatric patient-derived neurons have uncovered disease-, endophenotype-, and in some cases gene-associated cellular phenotypes such as progenitor cell proliferation, morphological maturation, synaptic connectivity, and neuronal activity [8]. SCZD was among the first psychiatric disorders to be studied using patient iPSCs, wherein idiopathic patient-derived neurons were found to display decreased neuronal connectivity, spine density, and synapses in vitro [9]. Given the strong implication of dopaminergic dysregulation in SCZD pathogenesis, another study found delayed maturation, reduced dopamine release, and mitochondrial dysfunction in patient iPSC-derived dopaminergic neurons [10]. For bipolar disorder (BPD), a study using iPSCs from two siblings with BPD compared to neurotypical parents as controls revealed defects in neuronal differentiation as well as differential expression of genes involved in calcium binding, neuronal differentiation, and cellular phenotypes [11]. Using lithium-responsive and non-responsive cohorts, phenotypes of hyperexcitability, specifically in patient-derived dentate gyrus-like neurons, and altered expression of genes regulating mitochondrial function, neuronal excitability, and calcium signaling have been observed [12]. In addition to providing disease models and disease-relevant assay systems, iPSC technology has the potential to enable drug screening using patient-derived neural subtypes in vitro. Thus far, there have been no studies on MDD or treatment resistance in MDD using patient-derived neurons in vitro.

In our study, to generate iPSCs we selected robust cases of SSRI-responsive (remitters, R) and SSRI-resistant (nonremitters, NR) patients from a larger cohort of well-characterized MDD patients. SSRIs acutely increase serotonin levels by binding to the serotonin transporter with high affinity and blocking reuptake of serotonin (5-HT) by serotonergic neurons. Although it remains unclear how increased 5-HT levels translate to therapeutic benefits in humans, serotonergic neurotransmission in target regions in the forebrain, such as the cortex and hippocampus, may play a role in mediating the therapeutic actions of SSRIs. Following SSRI treatment, serotonin concentrations increase at postsynaptic sites in target brain regions, but it remains unclear what downstream cellular effects are associated with and, therefore, might contribute to, SSRI resistance in MDD patients. In our study, we specifically sought to study postsynaptic serotonergic neurotransmission in patient neurons. Mimicking the action of SSRIs, we examined the activity responses of patient-derived neurons to extracellular 5-HT. 5-HT caused hyperactivity in NR neurons in contrast to what was observed in neurons from neurotypical and R groups. We found that the 5-HT-induced hyperactivity was downstream of upregulated expression of 5-HT2A and 5-HT7 receptors. Pharmacological blockade of these receptors partially rescued 5-HT-induced hyperactivity in NR patient-derived neurons. We further tested a clinically relevant compound, Lurasidone, a high-affinity antagonist of 5-HT2A and 5-HT7 receptors and found that it was sufficient for blocking 5-HT-induced hyperactivity in NR neurons. We provide evidence for in vitro cellular and molecular mechanisms associated with SSRI resistance, and our findings indicate that 5-HT2A and 5-HT7 receptors may serve as targets for treating depression in SSRI-resistant patients. Our data suggest that altered serotonergic neurotransmission is associated with SSRI resistance, and 5-HT-induced hyperactivity in forebrain regions may play a role in setting up maladaptive neural circuits associated with SSRI resistance possibly in a subset of MDD patients.

Results

Deriving iPSCs from a cohort of SSRI-R and SSRI-NR patients

A cohort of 803 patients with MDD were taken off of all prior medication and started on an 8-week SSRI regimen of either Citalopram or Escitalopram as part of the Pharmacogenomic Research Network Antidepressant Medication Pharmacogenomic Study (PGRN-AMPS) [13]. All patients were scored for depressive behaviors using the quick inventory of depressive symptomatology (QIDS) and Hamilton depression (HAMD) rating scales before the start of treatment and after 8 weeks of SSRI treatment. From this cohort, extreme cases of SSRI responders and non-responders were selected for further study and skin biopsies.

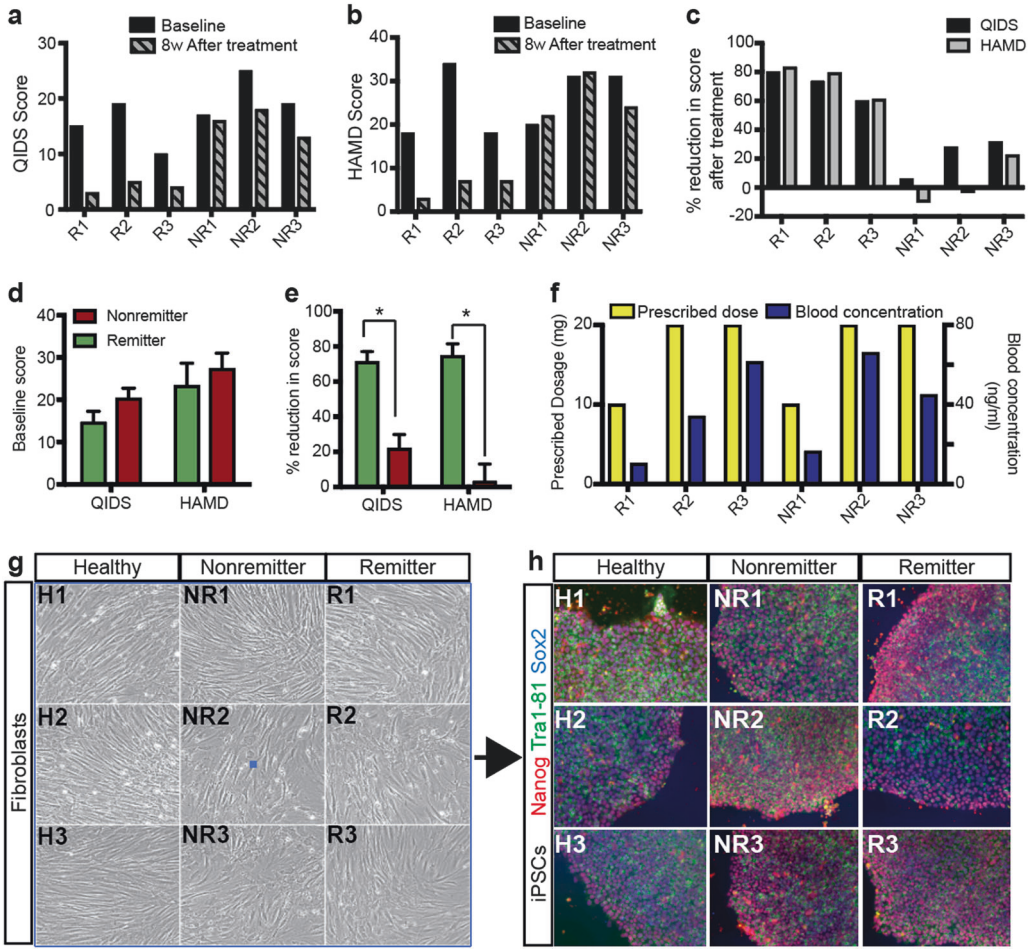

Fig. 1 Selective serotonin reuptake inhibitor (SSRI)-remitter (R) and SSRI-nonremitter (NR) patient characterization and induced pluripotent stem cell (iPSC) generation. Three SSRI-R (R1–R3) and SSRI-NR (NR1–NR3) patients were selected from a larger cohort for further characterization and iPSC generation. **a**, **b** Quick inventory of depressive symptomatology (QIDS) and Hamilton depression (HAMD) scores of individual major depressive disorder (MDD) patients at baseline (black bars) and after 8 weeks of SSRI treatment (gray striped bars). **c** Percentage reductions in QIDS (yellow bars) and HAMD (blue bars) scores in individual patients after 8 weeks of SSRI treatment. **d**, **e** Group averages of **d** baseline and **e** percent reduction of QIDS and HAMD scores for R (green bars) and NR (red bars) groups. **f** Patients were prescribed SSRI dosage of 10 (Escitalopram) or 20 mg (Citalopram) (gray bars, left *y*-axis) and blood concentration of SSRIs (black bars, right *y*-axis) was measured 8 weeks after treatment. **g** Brightfield images of fibroblasts derived from skin biopsies of three healthy neurotypical controls (H1–H3), three NRs (NR1–NR3), and three Rs (R1–R3). **h** Fibroblasts were reprogrammed to iPSCs and shown are representative overlay images of iPSC colonies immunopositive for pluripotency markers nanog (red), tra1-81 (green), and sox2 (blue). One iPSC clone per individual was used for experiments. Graphs represent mean values ± SEM (error bars). **p* Value < 0.01 from comparing averages from groups (three individuals per group) using unpaired *t*-test with Welch's correction in **e**

Only patients who achieved remission after SSRI treatment were considered to be R; those with nonsignificant improvements in QIDS and HAMD scores were considered to be NR (Fig. 1) (Supplementary Table 1). Prior to SSRI treatment, R and NR groups displayed comparable QIDS and HAMD scores, indicating equal severity of MDD symptomatology, but they exhibited significantly different percent reductions in QIDS and HAMD scores 8 weeks after treatment (Fig. 1a, b, d). Rs displayed substantial (~70%) reductions in depressive scores, whereas NRs displayed minor reductions (~20%), if any, following SSRI treatment (Fig. 1c, e). In both groups, patients were prescribed either 10 or 20 mg of the SSRI escitalopram or citalopram (Fig. 1f, Supplementary Table 1), and no significant differences were observed in the blood concentration of SSRIs between groups (Fig. 1f). To rule out the possibility of differences in drug processing peripherally, we plotted the correlation between SSRI blood concentrations and therapeutic improvement after treatment. We found no correlation between blood SSRI concentrations and reduction in depressive scores among MDD patients (Supplementary Figure 1). Skin biopsies were performed on 3 R patients, 3 NR patients, and 3 healthy (H) individuals without a history of depression (Fig. 1g), and their fibroblasts were obtained for reprogramming (Fig. 1g). Skin fibroblasts were reprogrammed with viral vectors

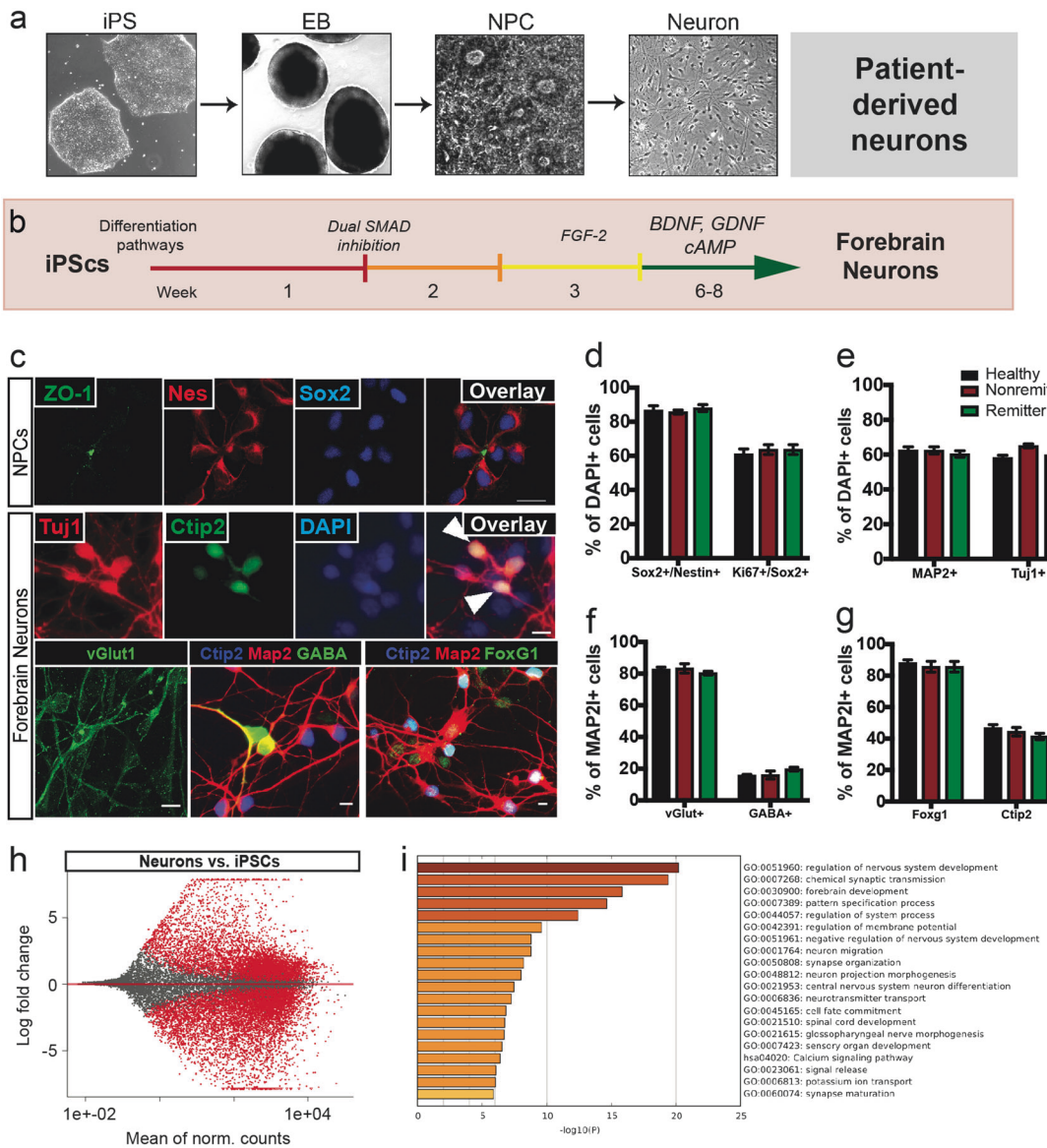

Fig. 2 Generating forebrain neurons from patient-derived induced pluripotent stem cells (iPSCs). **a** Brightfield images are examples of patient-derived cells at different stages in the process of neuronal differentiation, from iPSCs to embryoid bodies (EBs), to neural precursor cells (NPCs), to neurons. **b** Schematic depicts method and timeline for generating human forebrain neurons by dual SMAD pathway inhibition and fibroblast growth factor-2 activation for differentiating neurons from patient iPSCs. **c** (Upper panel) Representative fluorescence images of patient NPCs immunopositive for markers —ZO-1 (green), Nestin (red), and Sox2 (blue). **c** (Middle panel) Examples of confocal fluorescence images of differentiated patient neurons expressing neural and cortical markers: Tuj1 (red), Ctip2 (green), and DAPI+ (blue) nuclei; (lower panel) overlay examples of iPSC-derived vGlut1+ (green) neurons; and Ctip2+ (blue), Map2+ (red), and GABA+ (green) double-positive neurons; and Ctip2+ (blue), Map2+ (red), and Foxg1+ (green) double-positive neurons. Arrowheads indicate double-positive cells. **d** Quantification shows a high percentage of NPCs (DAPI+ nuclei) to be double-positive for markers of neural fate (Sox2 and Nestin) and proliferation (Ki67 and Sox2). **e** Quantification shows a high percentage of neuronal differentiation assessed using Map2 and Tuj1 markers. **f** Graph shows percentage differentiation into glutamatergic (vGlut1+) and GABAergic (GABA+) neurons, and **g** a majority of neurons also expressing the forebrain and cortical markers Foxg1 and Ctip2. **h** Shown is an MA-plot of the transcriptome of all patient-derived neurons vs. patient iPSCs and red dots represent significant differentially regulated genes. **i** Gene ontology analysis of the top 500 upregulated genes (fold change and significant) in all patient-derived neurons vs. iPSCs, with a list of the most significant gene ontology categories. Scale bars represent 20 μm (**c**, top panel), 10 μm (**c**, middle and lower panels). Graphs represent mean values calculated from three independent differentiation experiments ± SEM (error bars)

expressing reprogramming transcription factors (Fig. 1h) to generate iPSCs. Karyotypically normal iPSC clones that passed quality control criteria and expressed pluripotency markers were selected for deriving neurons for functional experiments (Supplementary Figure 2). One clone per individual was selected for further experiments.

Generating forebrain neurons from patient-derived iPSCs

In vitro tools offer the unique advantage of permitting the study of distinct and disease-relevant cellular subtypes, which is often difficult to do in vivo. In the context of studying serotonergic neurotransmission in target brain regions, we specifically sought to examine the effects of 5-HT on patient iPSC-derived forebrain neurons (Fig. 2). Embryoid bodies (EBs) generated from patient iPSCs were exposed to neuralizing and fate-specifying patterning cues for generating neural precursor cells (NPCs) and forebrain neurons (Fig. 2a, b). Patient-derived NPCs were immunopositive for the NPC markers Nestin and Sox2 and displayed characteristic polar distribution of the apical tight-junction marker ZO-1 (Fig. 2c, d). Quantification revealed that most of the iPSC-derived forebrain NPCs were double-positive for Nestin and Sox2, and a subset (~60%) were also proliferating, as observed using the endogenous marker, Ki67 (Fig. 2d). Following differentiation, we observed that patient-derived forebrain neurons were immunopositive for the neural markers MAP2ab and Tuj1 (~60%) (Fig. 2e). Typically, neuronal cultures derived from NPCs end up differentiating into both neurons and glial cells, enabling neurons to grow, survive, and remain active over long periods of time. We observed similar percentages of neurons and glial cells between groups (Fig. 2e; data not shown). A majority of the neurons, nearly 80%, were glutamatergic, expressing the marker vGLUT, and a smaller subset, <~20%, was GABAergic (GABA+) (Fig. 2f). Further characterization of patient iPSC-derived forebrain neurons revealed that the neurons expressed cortical markers to varying percentages, with over 80% being immunopositive for Foxg1 (>80%) and Ctip2 (~40%) (Fig. 2g). Notably, we observed similar percentages of markers between the three groups, with no significant differences (Fig. 2d–g). To further examine the differentiation of patient-derived neurons, we analyzed the whole transcriptome of all patient iPSCs and neurons by RNA sequencing and found a large number of genes to be significantly different between these cell types (>14,200; ~6600 up in neurons vs. iPSCs) (Fig. 2h). Unbiased gene ontology (GO) analysis of the top 500 significantly upregulated genes, based on fold change, revealed key GO terms such as "nervous system development," "forebrain development," and "pattern specification." These cells also expressed genes related to key pathways involved in neural signaling and neurotransmission, as observed by GO categories such as "regulation of membrane potential," "neurotransmitter transport," and "synapse maturation" (Fig. 2i). This suggested that not only did the iPSC-derived neurons express key forebrain marker genes, but actually adopted a forebrain fate as shown by gene expression pattern. Our data show that we successfully generated patient forebrain neurons with a high percentage of neurons also immunopositive cortical markers.

5-HT induces hyperactivity in SSRI-NR patient-derived neurons

Most forebrain regions are heavily innervated by serotonergic fibers and many cortical regions are postsynaptic targets of serotonergic innervation. Meta-analyses of magnetic resonance imaging (MRI) studies of over 2000 MDD patients revealed structural alterations in several brain regions [14]. Another study using functional MRI data from more than 1000 depressed patients found altered functional activity in frontostriatal and limbic circuits, on the basis of which patients could be subdivided into four neurophysiological subtypes [14]. The frontostriatal network includes the prefrontal, orbitofrontal, and anterior cingulate cortical forebrain regions, which heavily interact with limbic structures and are involved in executive functions and motivation. This evidence led us to ask whether differences in patient neuron activity might be associated with MDD. We examined neuronal activity using the calcium (Ca^{2+}) responsive and cell permeating dye Fluo-4 (Fig. 3a). In neurons, action potentials regulate Ca^{2+} levels through voltage-gated Ca^{2+} channels, and imaging the temporal dynamics of intracellular Ca^{2+} is widely used for studying neuronal spiking activity of local neuronal circuits in vitro and in vivo. First, we examined baseline activity in patient neurons (Fig. 3b). Following incubation with Fluo-4, we were able to observe and measure Ca^{2+} transients (spikes) in patient neurons over a period of 3 min (Fig. 3a, Supplementary video 1). We observed a distribution in the number of Ca^{2+} transients per individual at baseline, with some exhibiting single Ca^{2+} spikes and others exhibiting multiple spikes, however we found no significant differences between H (neurotypical healthy controls), NR, and R groups (Fig. 3b; Supplementary videos 2–4).

Given that SSRIs acutely increase 5-HT levels in target regions, including the cortex, we next sought to model the acute effects of SSRI treatment (Fig. 3c–g). To model actions of SSRI treatment, we examined neuronal activity of iPSC-derived neurons in response to exogenous 5-HT, which increases downstream of SSRI treatment (Fig. 3c–g). To study how 5-HT regulated neural activity, we performed a dose response curve and quantified neuronal activity at different concentrations of 5-HT (Supplementary Figure 3), and found 50 µM to be a dose at which postsynaptic calcium transients could be observed robustly. In this experiment, we observed that 5-HT caused an increase in the activity of individual patient-derived neurons and differentially regulated neuronal activity between the patient groups (Fig. 3c, d). Interestingly, NR forebrain neurons displayed

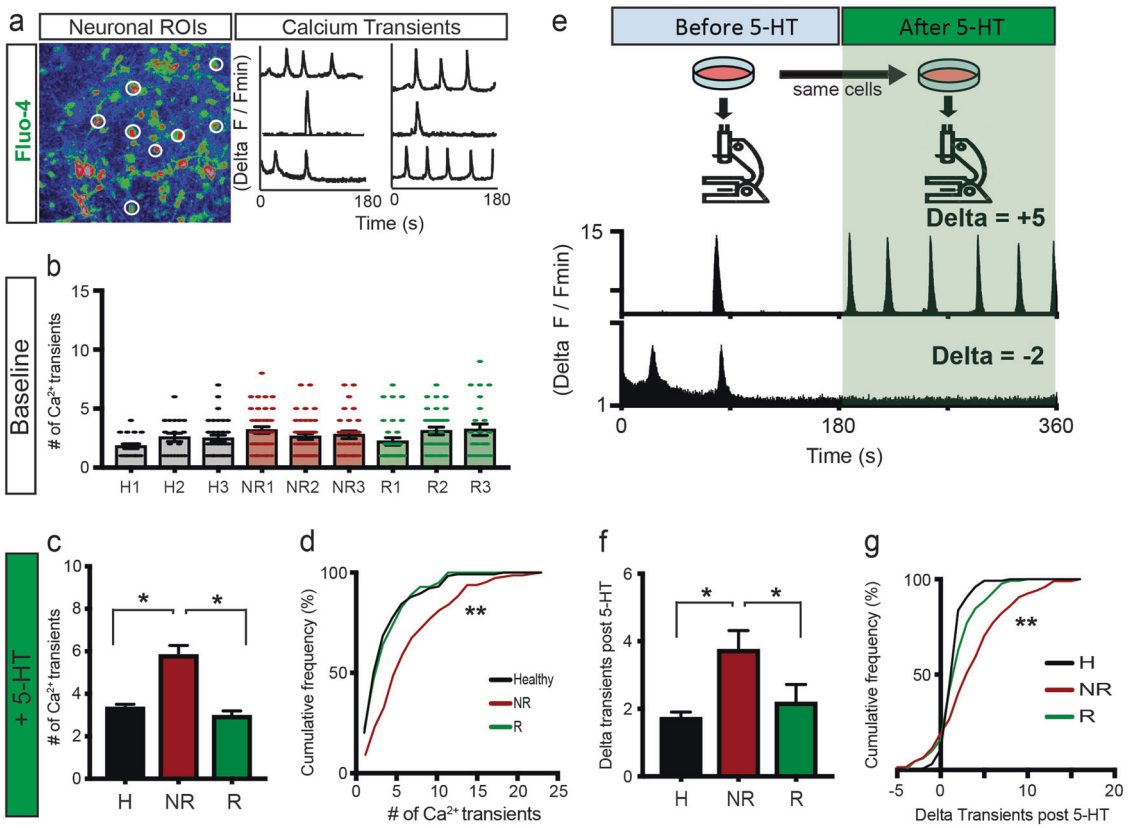

Fig. 3 5-HT-induced activity in patient induced pluripotent stem cell-derived neurons. **a** (Left panel) False color intensity image example of patient-derived neurons loaded with the Ca^{2+} indicator Fluo-4 with examples of labeled regions of interest (ROIs) outlined (white circles). **a** (Right panel) Examples of Ca^{2+} transients plotted as change of fluorescence intensity over a period of 3 min. **b** The distribution of the number of Ca^{2+} transients over 3 min in individual neurons per patient revealing no significant difference between H, NR, and R groups under baseline conditions. **c** Group averages and **d** cumulative frequencies of the number of calcium transients over 3 min after 5-HT treatment per patient group, with significantly higher average in NR vs. H and R groups. **e** Schematic depicts the experimental design for measuring change in neural activity in individual neurons after 5-HT treatment and shows derivation of the delta metric by subtracting the number of Ca^{2+} transients before 5-HT treatment from the number after 5-HT treatment. **f** Group average and **g** cumulative frequency of delta calcium transients after 5-HT treatment per patient group, with significantly higher averages in NR vs. H and R groups. Graphs represent mean values ± SEM (error bars). *p Value < 0.05 from comparing averages from three individuals in each group using Mann-Whitney test (unpaired, one-tailed) in **c** and **f**. For statistically comparing distribution of number of calcium transients (**d**) and delta calcium transients in **g**, values from three individuals were pooled and compared using the Kruskal-Wallis test, corrected for multiple comparisons with the two-stage method for false discovery rate (Benjamini, Krieger, and Yekutieli), **$p < 0.0001$

significantly higher activity, on average and as a distribution, when compared to Hs and Rs following 5-HT treatment, whereas no significant differences between H and R groups were observed (Fig. 3c, e; Supplementary Figure 3; Supplementary videos 5–7). These results showed that although baseline activity did not differ between groups, 5-HT induced increased activity specifically in NR patient-derived neurons.

From our analyses, we observed that there was a wide distribution in the number of Ca^{2+} transients within the population of neurons, leading us to more deeply examine how individual neurons responded to 5-HT. We performed live Ca^{2+} imaging of the same populations of neurons prior to and after 5-HT treatment (Fig. 3e). In these experiments we were able to quantify the number of Ca^{2+} transients before and after treatment in the same set of neurons (Fig. 3e). We devised a delta metric in which we subtracted the number of Ca^{2+} transients under baseline conditions from the number observed after 5-HT for each individual neuron. The delta metric gave us a normalized binary measure with which to quantify change in neuronal activity after 5-HT treatment in populations of individual neurons (Fig. 3e). Positive delta values meant an increase in the number of Ca^{2+} spikes and negative delta values indicated a relative decrease per neuron post 5-HT treatment. In this experiment, on average we found positive delta values across all individual patient-derived neurons, suggesting that on average 5-HT increased activity in neurons in vitro (Fig. 3f). We observed significantly higher average delta values and higher cumulative percentages in NR patient neurons as compared to Hs and Rs (Fig. 3f, g; Supplementary Figure 3; Supplementary videos 5–7). These data

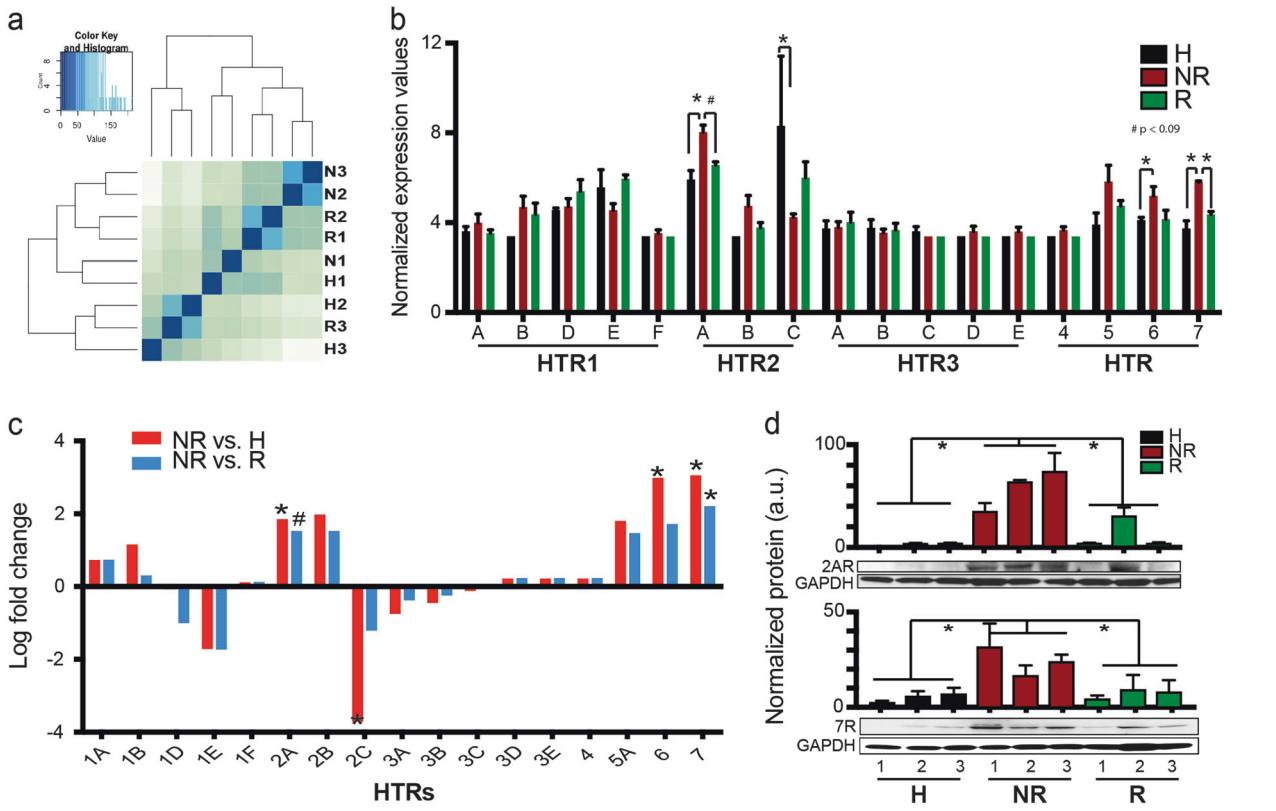

Fig. 4 Altered 5-HT receptor levels in patient induced pluripotent stem cell-derived neurons. **a** Heatmap of unsupervised hierarchical clustering of whole transcriptome of patient forebrain neurons. **b** From whole transcriptome plotted normalized expression values of individual 5-HT receptors (*HTR1-7*). **c** Plotted are fold changes in expression of all 5-HT receptor genes (*HTR1-7*) in NR vs. R (blue bars) or H (red bars). **d** Representative blots and quantification of 5-HT2 (2AR) and 5-HT7 (7R) receptors normalized to GAPDH (GP) in patient neurons, showing significantly higher levels on average between NR vs. H and R groups. **b**, **c** Graphs represent mean values ± SEM (error bars) from three individuals per group, $*p$ value < 0.05, $^{\#}p$ value < 0.09. **d** Bars represent averages from technical triplicates per sample. Groups were statistically compared by averaging values of three individuals per group using unpaired *t*-test with Welch's correction, $*p < 0.05$

showed that when looking at individual neurons, a majority of which were forebrain glutamatergic neurons (Fig. 2), a higher percentage of NR neurons displayed 5-HT-induced hyperactivity. Our results suggested that 5-HT-induced neural hyperactivity might in part be associated with SSRI resistance. We next sought to explore the molecular mechanisms underlying this phenomenon.

Increased 5-HT2A and 5-HT7 receptor levels in NR patient neurons

5-HT mediates its direct effects on neurons via seven known families of serotonergic receptors, resulting in postsynaptic excitation or inhibition. Human genetic studies and preclinical studies have implicated different serotonergic receptors in MDD pathology as well as SSRI resistance. Given that 5-HT increased activity of NR neurons, we hypothesized that altered activity might occur downstream of altered 5-HT receptor levels in patient-derived neurons. To examine this hypothesis in an unbiased manner, we performed RNA sequencing and analyzed the whole transcriptome of patient-derived neurons while focusing on 5-HT receptor expression levels (Fig. 4a–d). First, we performed quality control and asked whether there were large differences between the transcriptomes of H, NR, and R patient forebrain neurons. With unsupervised hierarchical clustering and principal component analysis, we observed that patient groups did not segregate on the basis of disease status or SSRI responsiveness (Fig. 4a; Supplementary Figure 4), suggesting that, on the whole, neurons derived from each patient group did not differ extensively. We observed that a small number of genes significantly differed between H and R groups (H vs. R = 36 genes), and the largest number of differentially regulated genes were observed when comparing NR to both other groups (NR vs. R = 163 genes) (Supplementary Figure 4). Given that 5-HT increased activity specifically in NRs compared to both other groups, we hypothesized that it was possible that alterations in serotonin receptor genes could directly contribute to the observed differences in NRs vs.

both other groups. We examined expression of the 17 5-HT receptor genes in MDD patient-derived neurons (Fig. 4b). Strikingly, 4 serotonergic receptors—*HTR2A*, *HTR2C*, *HTR6*, and *HTR7*—were differentially regulated in NR vs. H groups (Fig. 4b). Two serotonin receptors showed differential expression in NR vs. R groups, *HTR7* was significantly different and *HTR2A* showed a trend ($p < 0.09$) toward differential regulation (Fig. 4b, d). In examining the fold changes of 5-HT receptor gene expression in NR vs. both other groups, we found that expression of both *HTR2A* and *HTR7* was nearly fourfold higher in NR neurons compared to H and R groups (Fig. 4c). It is noteworthy that the upregulated 5-HT receptors, 5-HT2A and 5-HT7, are both excitatory G-protein coupled receptors (GPCRs) and cause excitatory postsynaptic action potentials upon stimulation with 5-HT. To confirm our observations, we asked whether the differences in 5-HT receptor transcript levels translated to differences in 5-HT receptor protein levels. Western blotting from lysates of differentiated patient forebrain neurons revealed significantly higher levels of 5-HT2A and 5-HT7 receptor protein in NR neurons compared to both H and R groups (Fig. 4d). This observation was specific to 5-HT2A and 5-HT7 receptors, as we did not find group differences in protein levels of other serotonergic receptors such as the 5-HT1AR and 5-HT5R (Supplementary Figure 5). These results corroborated our transcriptomic data. Considering that both 5-HT2A and 5-HT7 receptors are excitatory GPCRs, these data raised the possibility that 5-HT may be mediating its downstream effects at least in part via the 5-HT2A and 5-HT7 receptors. This led us to ask whether there was a correlation between 5-HT-induced activity and expression levels of 5-HT2A or 5-HT7 receptors. Strikingly, we observed a significant correlation between *HTR2A* receptor expression and delta activity post 5-HT (Supplementary Figure 6) and a trend with *HTR7* expression, suggesting that 5-HT-induced activity changes in NR patient-derived neurons were likely downstream of increased 5-HT2A and 5-HT7 receptors.

Antagonists of 5-HT2A and 5-HT7 receptors block 5-HT-induced hyperactivity in NR patient-derived neurons

To examine the role of 5-HT2A and 5-HT7 receptors in mediating the postsynaptic effects of 5-HT in patient neurons, we next asked whether pharmacological blockade of these receptors would prevent 5-HT-induced hyperactivity in NR patient neurons (Fig. 5). For this set of experiments, patient neurons were pretreated with either vehicle or specific receptor antagonists and then incubated with Fluo-4 for live Ca^{2+} imaging for 3 min prior to and after the addition of 5-HT (Fig. 5a). As previously described, the same populations of neurons were examined before and after

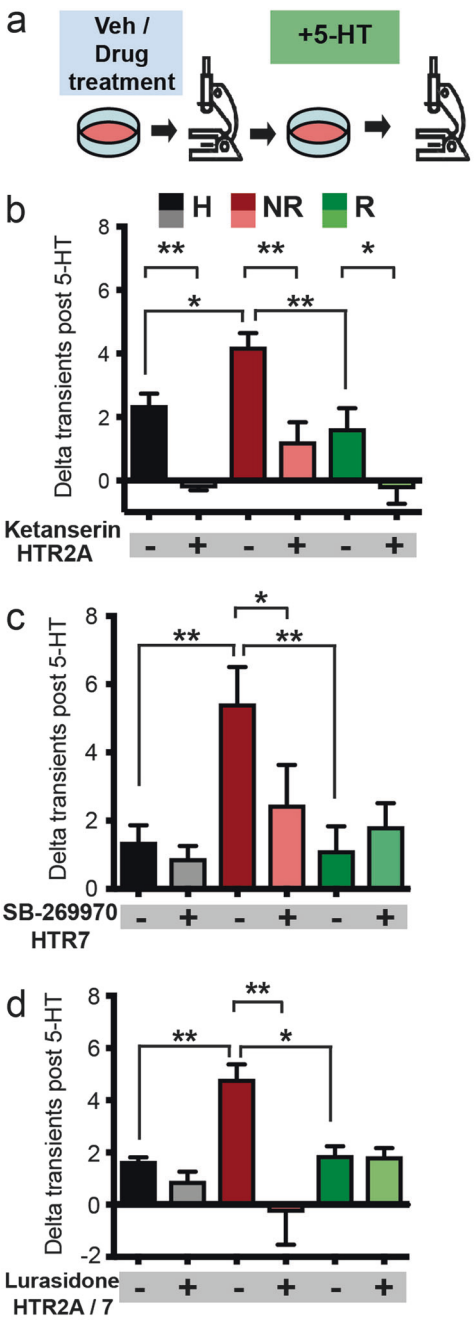

e

Activity Post 5-HT			
Condition	H	NR	R
No Drug	↑↑	↑↑↑	↑↑
Ketanserin	↑	↑↑	↑
SB-259970	↑	↑↑	↑
Lurasidone	↑	↑	↑

5-HT treatment, and a change in the number of Ca^{2+} transients was quantified using the delta metric (Fig. 2a). In separate experiments, we used Ketanserin, a high-affinity

◀ **Fig. 5** Pharmacological blockade of 5-HT2 and 5-HT7 receptors rescues 5-HT-induced hyperactivity in nonremitter (NR) patient neurons. **a** Schematic depicts experimental design for studying pharmacological blockade of 5-HT-induced neural activity. Patient neurons were pretreated with Ketanserin (5-HT2AR antagonist), SB-269970 (5-HT7R antagonist), or Lurasidone or vehicle (phosphate-buffered saline), followed by live Ca^{2+} imaging, before and after 5-HT treatment. Change in neural activity was quantified using the delta metric in the same populations of neurons. **b** Quantification of Ketanserin-pretreated H, NR, and R neurons showed significantly lower delta values compared to vehicle-treated controls. **c** SB-269970-pretreated NR group had lower delta values as compared to vehicle-treated controls (5-HT7R block). **d** Lurasidone significantly lowered delta values in the NR group as compared to vehicle-treated group. **e** Summary table shows directionality (black arrows) of change in activity following 5-HT treatment in H, NR, R groups under baseline conditions and with the different antagonists, as listed. Graphs represent mean values ± SEM (error bars) from three individuals per group. Groups were compared statistically using two-way analysis of variance and Fisher's least significant difference test for multiple comparisons. *p Value < 0.05, **p value < 0.01

5-HT2A receptor antagonist, and SB-269970, a high-affinity 5-HT7 receptor-specific antagonist. First, with Ketanserin pretreatment, we found that across all three groups, Ketanserin significantly blunted 5-HT-induced activity (Fig. 5b). Notably, NR neuron hyperactivity was significantly reduced with Ketanserin pretreatment, with the change in activity now being comparable to H and R vehicle-treated groups (Fig. 5b). Similarly, 5-HT7 receptor blockade with SB-269970 significantly blunted 5-HT-induced hyperactivity in NR neurons, making them comparable to H and R vehicle-treated groups (Fig. 5c; Supplementary videos 8–10). These data showed that of 5-HT2A and 5-HT7 receptors each mediated 5-HT-induced hyperactivity in NR patient-derived neurons and that pharmacological blockade of these receptors rescued the hyperactivity phenotype.

To explore the potential clinical relevance of our findings, we asked whether a Food and Drug Administration (FDA)-approved compound with high affinity and antagonistic properties for both 5-HT2A and 5-HT7 receptors would be able to also block 5-HT-induced hyperactivity in NR patient-derived neurons. Our search led us to Lurasidone, an antipsychotic drug also prescribed for BPD, that among other receptors also binds to the 5-HT2A and 5-HT7 receptor [15]. Lurasidone is a high-affinity antagonist for each of the receptors: 5-HT2A, Ki = 2 nM and 5-HT7, Ki = 0.5 nM. Hence, in the same experimental paradigm we tested whether Lurasidone blocked 5-HT-induced activity in patient-derived neurons. We found that Lurasidone pretreatment significantly blunted 5-HT-induced hyperactivity in NRs, making them comparable to Lurasidone-treated H and R groups (Fig. 5d, Supplementary video 10). These results indicate that 5-HT-induced hyperactivity in NR neurons was at least partially mediated via both 5-HT2A and 5-HT7 excitatory serotonergic receptors, and blockade of these receptors by multiple antagonists including a clinically used drug was able to rescue this in vitro phenotype associated with SSRI resistance (Fig. 5e).

Discussion

In our study, we have focused on specifically examining mechanisms of SSRI resistance in MDD by generating neurons from patients at the extreme ends of the SSRI response spectrum. By isolating the postsynaptic compartment of serotonergic neurotransmission and examining responses to 5-HT, we were able to discover that NR patient-derived neurons displayed 5-HT-induced hyperactivity via upregulated 5-HT2A and 5-HT7 receptors.

Our data suggest that SSRI-resistant patients represent a subset of MDD patients with differential responses to 5-HT, but how the 5-HT-induced hyperactivity in vitro correlates with brain activity in vivo remains to be explored. Based on our findings and the fact that 5-HT is present in the brain under normal conditions, we hypothesize that SSRI-resistant patients may display increased activity in brain regions that are a target of serotonergic innervation, such as the cortex and hippocampus. While a limited number of studies have imaged brain activity specifically in SSRI-Rs vs. NRs, several reports indicate increased activity in limbic and cortical brain regions of subsets of MDD patients [16]. In a study by McGrath et al., a cohort of 46 MDD patients were enrolled in a two-phase treatment study with 12 weeks of Citalopram treatment and/or cognitive behavioral therapy (CBT) followed by flurodeoxyglucose positron emission tomography scan. The data demonstrated that subcallosal cingulate cortex (SCC) metabolism was significantly higher in nonresponders (9 patients) than in remitters (36 patients) [17]. Their study concluded that pre-antidepressant metabolic brain states, with hyperactivity in the SCC and the superior temporal sulcus, might help identify nonresponse to standard antidepressant treatments. Further, replicated findings indicate hyperactivity of the SCC among patients refractory to multiple treatment modalities, including CBT and electroconvulsive therapy [18]. Several imaging studies provide evidence for increased cerebral blood flow and metabolism in forebrain regions, including the cortex (medial prefrontal cortex, dorsal anterior cingulate gyrus, dorsolateral prefrontal cortex), para hippocampal cortex, amygdyla, and medial thalamus, in depressed vs. control or remitted individuals [19]. However, due to the heterogeneous nature of MDD as well as the dynamic nature of brain activity, defining a robust imaging signature of the depressed or SSRI-resistant brain has remained challenging.

In vitro, NR patient neurons displayed hyperactivity in response to 5-HT via upregulated 5-HT2A and 5-HT7

receptors. Both 5-HT2A and 5-HT7 receptors have previously been implicated in MDD [20]. Despite variability among studies, GWA studies of depressed patients have found MDD- and antidepressant response-associated variants in the *HTR2A* gene, and some postmortem studies showed altered 5-HT2A receptor levels in the brains of MDD patients [21, 22]. Our data provide new evidence supporting the idea that intrinsic increases in 5-HT2A forebrain receptors and downstream hyperactivity may be a primary phenotype preceding SSRI resistance possibly in a subset of SSRI-resistant individuals. Given that our cohort comprised only of women, the data must be extrapolated to a larger and more diverse patient population with caution.

In the clinic, most atypical antidepressants such as Nefazodone (Ki = 26 nM), Mirtazepine (Ki = 69 nM), and Trazodone (Ki = 36 nM) have been found to be high-affinity antagonists of the 5-HT2A receptor [23–25]. Rodent studies indicate that 5-HT2A receptor blockade may prevent the emergence of behavioral and transcriptional alterations in early-life stressor-based models of depression [26] and antagonism of 5-HT2A receptors may have a synergistic effect to enhance the efficacy of SSRI treatment in patients [27]. Similarly, 5-HT7 receptor knockout mice and 7R antagonist-treated mice display antidepressant-like behavior and in rats antidepressants themselves may act by regulating 5-HT7 receptor levels in vivo [28, 29]. Clinically, a more recently used atypical antidepressant, Vortioxetine, has also been found to be an antagonist of the 5-HT7 receptor (Ki = 19 nM) [30]. In conjunction with these studies, our data raise the possibility that drugs that act as antagonists at either or both 5-HT2A and 5-HT7 receptors may have therapeutic value as antidepressants for treating SSRI-resistant patients. Furthermore, our data suggest that Lurasidone and other FDA-approved antagonists of the 5-HT2A and 5-HT7 receptors could be repurposed for treating SSRI-resistant MDD. However, it is important to note that both Ketanserin and Lurasidone also bind to other 5-HT receptors with high affinity (Ketanserin for 5-HT2B at Ki = 2 nM, 5-HT2C at Ki = 30 nM, and Lurasidone for 5-HT1A at Ki 7 nM). Given that we used these pharmacological antagonists at higher concentrations than their Ki values for 5-HT2A and 7 receptors, it is possible that 5-HT-induced hyperactivity in NR neurons is entirely not limited to 5-HT2A and 5-HT7 receptors. Separately, regarding the interpretation of our results from SSRI-responsive patient-derived neurons, the possibility of spontaneous improvement over time regardless of antidepressant treatment must be considered while interpreting our data.

There are several caveats to the iPSC-neural model system, including low throughput and high variability, which must be kept in mind while interpreting data [31] specifically because we have a small number of patients per group. To partially address this issue, in our study we utilized the extreme pharmacological phenotype to segregate our patients to uncover novel phenotypes in vitro. iPSC-derived neurons are still relatively immature, so it remains to be ascertained how acute, in vitro phenotypes correlate with brain activity in adult patients in vivo. Nonetheless, our data provide evidence for the hypothesis that altered postsynaptic serotonergic neurotransmission in forebrain neurons, downstream of 5-HT-induced hyperactivity, may result in maladaptive circuitry, giving rise to SSRI resistance, at least in a subset of MDD patients. Our results paint a complex and more nuanced picture of the serotonergic hypothesis of depression and highlight a role for serotonergic dysfunction in the neuropathology of SSRI resistance in MDD that can be studied further to understand treatment resistance.

Materials and methods

Subjects

MDD subjects were participants in the PGRN-AMPS (1-004134-07), as previously described [13]. Patients were adult females, between the ages of 33 and 53 with additional information listed in Supplementary Table 1. Treatment outcomes were determined using the HAMD-17 and QIDS-C16 [32] depression rating scales before the start of SSRI (20 mg of Citalopram or 10 mg of Escitalopram) treatment and 8 weeks after SSRI treatment (Supplementary Table 1). Patient blood samples were collected and drug levels measured as previously described [13]. SSRI-Rs and -NRs were selected based on treatment outcomes after 8 weeks in the PGRN-AMPS, and skin punch biopsies from subjects were obtained under sterile conditions for further studies. Risks and benefits were discussed with study participants, and all subjects provided written informed consent at the start of the study. All procedures were monitored and approved by the Institutional Review Board of the Mayo Clinic or the Salk Institute.

Generation of patient-derived iPSCs and neurons

Fibroblasts from punch biopsies of patients and healthy controls were cultured for reprogramming into iPSCs. Patient iPSCs were reprogrammed from primary human fibroblasts using Sendai virus within the CytoTune-iPS Sendai Reprogramming Kits according to the manufacturer's instructions (Invitrogen, A13780-02, A16517, A16518) and manufactured by ReGen Theranostics (Rochester, MN). Skin biopsies were undertaken in accordance with institutional regulations (Mayo Clinic IRB 10-006845). One iPSC line per patient was generated for characterization, for generating NPCs, and for neuronal

differentiation. iPSCs were confirmed to be karyotypically normal and characterized as previously described to express pluripotency markers (Supplementary Figure 1) [33]. iPSCs were cultured on Matrigel-coated plastic plates (BD Biosciences) using a modified recipe of mTeSR1 medium (Stemcell Technologies). Patient neurons were generated as previously described [33]. Briefly, floating EBs were generated by mechanical and enzymatic dissociation of iPSC colonies using collagenase and were transferred to low-attachment plates in neural induction media (NIM: DMEM/F12 containing N2 and B27 supplements, Thermo Fisher Scientific). EBs were maintained in NIM containing Noggin (100 ng/ml), LDN193189 (100 nM), and SB431542 (10 µM). After a week, EBs were transferred to poly-ornithine and laminin-coated plates in NIM containing fibrobast growth factor-2 (20 ng/ml) and laminin (1 µg/ml). Rosette-forming EBs were selected and dissociated using Accutase (Chemicon) and plated on polyornithine- and laminin-coated plates to generate NPCs. NPCs were maintained at high density as monolayers and were plated at lower densities for neuronal differentiation for 4 to 8 weeks. For neural differentiation, NPCs were switched to neural differentiation medium (NDM) containing brain-derived neurotrophic factor (20 ng/ml, Peprotech), glial cell-derived neurotrophic factor (20 ng/ml, Peprotech), dibutyrl-cyclic AMP (1 mM, Sigma), ascorbic acid (200 nM, Sigma), laminin (1 µg/ml), non-essential amino acids (1×, Sigma) in DMEM/F12-Glutamax:Neurobasal (1:1) + N2 + B27 base media. The medium was changed every other day for 3–8 weeks and antibiotic-antimycotic solution (1×, Sigma) was added for terminal experiments as needed. All cell lines were regularly verified to be free from mycoplasma contamination.

RNA preparation and sequencing analysis

For whole transcriptome analysis, 6- to 8-week-old neurons were harvested for RNA isolation. Total cellular RNA was extracted from approximately 3×10^6 cells using TriZol (Thermo Fisher Scientific) or RNA-Bee (Qiagen) according to the manufacturer's instructions. RNA-Seq libraries were prepared using the TruSeq Stranded mRNA Sample Prep Kit according to the manufacturer's instructions (Illumina) and reverse transcribed into cDNA with SuperScript II reverse transcriptase (Invitrogen). Stranded cDNA libraries were generated according to Illumina's procedures. Total (mRNA) RNA-Seq libraries were sequenced as single-end 50 basepairs using the Illumina® HiSeq 2500 platform according to the manufacturer's specifications. Low-quality ends and adapter removal/trimming were performed using cutadapt. Trimmed reads were mapped using STAR [34] and assigned to genes with featurecounts [35], and normalized counts and differential expression and statistics were calculated using the DESeq2 R package [36]. Normalized count numbers were processed using R software to plots for further analysis and visualization. RNA-sequencing data are available via a GEO accession code GSE125664.

Immunocytochemistry and western blotting

For immunocytochemistry, cells were plated on poly-ornithine/laminin-coated plastic slides and fixed with cold 4% paraformaldehyde solution for 15 min at 4 °C. Antigen blocking and cell permeabilization were done using 3% horse serum and 0.1% Triton X-100 in Tris-buffered saline for 30 min at 4 °C. Primary antibodies were incubated in the above-described blocking solution overnight at 4 °C. The primary antibodies used are listed in Supplementary Table 2. Following washes, fluorophore-coupled donkey secondary antibodies (1:250, Jackson Laboratories) were incubated in the blocking solution for 1 h at room temperature as previously described. The cells were counter-stained with 4′,6-diamidino-2-phenylindole for nuclei detection followed by washes and coverslipping in poly-vinyl alcohol mounting medium with DABCO (Sigma). Quantification of percent differentiations was performed manually, on average from three to five fields of view from three sets of differentiation experiments. Approximately, 450–800 cells were counted for determining percent differentiation from each patient-derived NPC line, as shown in Fig. 2.

For western blotting, 6- to 8-week-old neural cultures of approximately 3×10^6 cells were lysed into RIPA buffer (Thermo Scientific) containing protease and phosphatase inhibitors (Thermo Scientific) and incubated on ice for 5 min as previously described [37]. Lysates were clarified by centrifugation (14,000 rcf for 15 min at 4 °C), and western immunoblotting was performed following standard procedures using the iBlot gel and transfer system (Life Technologies). Briefly, blots were incubated in primary antibodies (sequentially) overnight at 4 °C, and, following washes, they were incubated in horseradish peroxidase-coupled secondary antibodies for 1 h at room temperature, followed by washes and enhanced chemiluminescence detection as per the manufacturer's instructions. Primary antibodies used for western blotting and immunocytochemistry are listed in Supplementary information.

Live calcium imaging and pharmacological treatment paradigms

Six- to 8-week-old iPSC-derived forebrain neurons were utilized for studying 5-HT-induced activity and blockade with serotonergic receptor antagonists. For imaging calcium transients in patient-derived neuronal cultures, we utilized

the cell permeable calcium binding dye Fluo-4 AM. Fluo-4 was prepared according to the manufacturer's instructions from the Fluo-4 calcium imaging kit (ThermoFisher scientific). Neuronal cultures were incubated with Fluo-4 (1 μM) for 15–20 min at 37 °C, following which cells were washed with NDM prior to imaging. Live imaging was performed using a spinning disk confocal microscope (Zeiss). Images were obtained were taken every 131 ms with the ×10 or ×20 objective for a period of 180 s. Fields of view were randomly but based on how clearly cell bodies were visible (Supplementary information). For live calcium imaging experiments, cells were plated at densities ranging from 40,000 to 80,000 cells/well of a slide and on average, <5% of cells were active in a given field of view for the 3 min duration of an imaging session. Comparable densities of cells were utilized for imaging experiments across lines, and four to five fields of view were imaged per line, per experiment, averaged over three experimental replicates. Approximately, 80–200 cells were quantified per line and averaged for data shown in Fig. 3. Neurons were outlined as individual regions of interest (ROIs) and analyzed using ImageJ software (http://imagej.nih.gov/ij/). For each ROI, change in fluorescence intensity over time (Delta F) was plotted and values were normalized to the minimum fluorescence (F min) for counting spikes or transients per ROI (Supplementary information). Active cells were defined based on spike pattern as determined by the Delta F (Fig. 3). Time-lapse images were quantified using raw data and representative videos have been uniformly sped up for visualization purposes. Neurons were incubated with Ketanserin (1 μM, Tocris), SB-269970 (10 μM, Tocris), Lurasidone (2 nM, Sigma), or vehicle (phosphate-buffered saline). All drugs were diluted to their final concentrations in NDM. Neurons were incubated with drugs at respective concentrations, following which they were incubated with Fluo-4, washed, and imaged as described above. Live Ca^{2+} imaging was performed before and after addition of 5-HT (50 μM, Sigma) to the culture medium, and activity was measured per neuron as described above.

Data analysis and statistics

Experiments were repeated as independent triplicates to obtain averages per individual per group for further statistical analysis. When comparing pairs of disease groups, statistical comparisons were performed by comparing average values from individuals (3) per group utilizing the following nonparametric statistical tests: unpaired one-tailed *t*-test with Welch's correction or Mann-Whitney test. For hypothesis testing as to whether observable differences in averages between groups were statistically significant, one-tailed *t*-tests were performed. In specific cases, when distribution of values was compared per group, values from all samples per group were pooled and compared using the Kruskal-Wallis test and corrected for multiple comparisons. Two-way analysis of variance was used for testing the interaction between two variables (disease and pretreatment) followed by Fisher's least significant difference for pairwise comparison between groups. Statistical tests and p values for individual experiments are stated in the figure legends, and $p < 0.05$ was considered statistically significant, and trending toward significance at $0.09 < p > 0.05$ (as stated in figure legends).

Acknowledgements This research was supported by Robert and Mary Jane Engman Foundation, Lynn and Edward Streim, Takeda-Sanford Consortium Innovation Alliance grant program (Takeda Pharmaceutical Company). KCV was supported by the Swiss National Science Foundation (SNSF) outgoing postdoctoral fellowship. Salk core facilities are supported by the Cancer center (NCI P30 CA014195). Patient enrollment and iPSC generation were funded by Minnesota Partnership Award for Biotechnology and Medical Genomics (YJ) and the 2012 Mayo Clinic Center for Regenerative Medicine (YJ). YJ was supported by the NIH-Mayo Clinic KL2 Mentored Career Development Award (NCAT UL1TR000135) and the Gerstner Family Mayo Career Development Award in Individualized Medicine. Patient recruitment and the laboratory aspects of the clinical trial were funded by NIH U19 GM61388 (PGRN) and NIH RO1 GM28157. The authors would also like to acknowledge the staff and investigators of the PGRN-AMPS study for their contributions, particularly the late Dr. David A. Mrazek, the former Principal Investigator of the PGRN-AMPS study within the Mayo Clinic NIH-PGRN (U19 GM61388). This research would not have been possible without Dr. Mrazek's pioneering vision and dedication to antidepressant pharmacogenomics research. We also thank Dr. Manching Ku for help with RNA sequencing, Galina Erikson for help with sequencing data, and ML Gage for editorial comments on the manuscript.

Compliance with ethical standards

Conflict of interest The authors declare that they have no conflict of interest.

Publisher's note: Springer Nature remains neutral with regard to jurisdictional claims in published maps and institutional affiliations.

References

1. http://www.who.int/mediacentre/factsheets/fs369/en/, http://www.nimh.nih.gov/health/statistics/prevalence/major-depression-among-adults.shtml, https://www.nlm.nih.gov/medlineplus/ency/article/000945.htm & http://www.dbsalliance.org/site/PageServer?pagename=education_statistics_depression
2. Vigo D, Thornicroft G, Atun R. Estimating the true global burden of mental illness. Lancet Psychiatry. 2016;3:171–8.
3. Kessler RC, Bromet EJ. The epidemiology of depression across cultures. Annu Rev Public Health. 2013;34:119–38.
4. Charney DS, Buxbaum JD, Sklar P, Nestler EJ. Neurobiology of mental illness. Oxford University Press: 2013.
5. Breen G, et al. Translating genome-wide association findings into new therapeutics for psychiatry. Nat Neurosci. 2016;19:1392–6.
6. Levinson DF, et al. Genetic studies of major depressive disorder: why are there no genome-wide association study findings and what can we do about it? Biol Psychiatry. 2014;76:510–2.

7. Wray NR et al. Genome-wide association analyses identify 44 risk variants and refine the genetic architecture of major depression. Nat Genet. 2018;50:668–81. https://doi.org/10.1038/s41588-018-0090-3
8. Soliman MA, Aboharb F, Zeltner N, Studer L. Pluripotent stem cells in neuropsychiatric disorders. Mol Psychiatry. 2017;22:1241–9.
9. Brennand KJ, et al. Modelling schizophrenia using human induced pluripotent stem cells. Nature. 2011;473:221–5.
10. Robicsek O, et al. Abnormal neuronal differentiation and mitochondrial dysfunction in hair follicle-derived induced pluripotent stem cells of schizophrenia patients. Mol Psychiatry. 2013;18:1067–76.
11. Madison JM, et al. Characterization of bipolar disorder patient-specific induced pluripotent stem cells from a family reveals neurodevelopmental and mRNA expression abnormalities. Mol Psychiatry. 2015;20:703–17.
12. Mertens J, et al. Differential responses to lithium in hyperexcitable neurons from patients with bipolar disorder. Nature. 2015;527:95–9.
13. Mrazek DA, et al. Treatment outcomes of depression: the pharmacogenomic research network antidepressant medication pharmacogenomic study. J Clin Psychopharmacol. 2014;34:313–7.
14. Drysdale AT, et al. Resting-state connectivity biomarkers define neurophysiological subtypes of depression. Nat Med. 2017;23:28–38.
15. Woo YS, Wang HR, Bahk WM. Lurasidone as a potential therapy for bipolar disorder. Neuropsychiatr Dis Treat. 2013;9:1521–9.
16. Ressler KJ, Mayberg HS. Targeting abnormal neural circuits in mood and anxiety disorders: from the laboratory to the clinic. Nat Neurosci. 2007;10:1116–24.
17. McGrath CL, et al. Pretreatment brain states identify likely non-response to standard treatments for depression. Biol Psychiatry. 2014;76:527–35.
18. Mayberg HS, et al. Deep brain stimulation for treatment-resistant depression. Neuron. 2005;45:651–60.
19. Price JL, Drevets WC. Neurocircuitry of mood disorders. Neuropsychopharmacology. 2010;35:192–216.
20. Artigas F. Serotonin receptors involved in antidepressant effects. Pharmacol Ther. 2013;137:119–31.
21. Kato M, Serretti A. Review and meta-analysis of antidepressant pharmacogenetic findings in major depressive disorder. Mol Psychiatry. 2010;15:473–500.
22. Hrdina PD, Du L. Levels of serotonin receptor 2A higher in suicide victims? Am J Psychiatry. 2001;158:147–8.
23. Anttila SA, Leinonen EV. A review of the pharmacological and clinical profile of mirtazapine. CNS Drug Rev. 2001;7:249–64.
24. Knight AR, et al. Pharmacological characterisation of the agonist radioligand binding site of 5-HT(2A), 5-HT(2B) and 5-HT(2C) receptors. Naunyn Schmiede Arch Pharmacol. 2004;370:114–23.
25. Cusack B, Nelson A, Richelson E. Binding of antidepressants to human brain receptors: focus on newer generation compounds. Psychopharmacology (Berl). 1994;114:559–65.
26. Benekareddy M, Vadodaria KC, Nair AR, Vaidya VA. Postnatal serotonin type 2 receptor blockade prevents the emergence of anxiety behavior, dysregulated stress-induced immediate early gene responses, and specific transcriptional changes that arise following early life stress. Biol Psychiatry. 2011;70:1024–32.
27. Marek GJ, Carpenter LL, McDougle CJ, Price LH. Synergistic action of 5-HT2A antagonists and selective serotonin reuptake inhibitors in neuropsychiatric disorders. Neuropsychopharmacology. 2003;28:402–12.
28. Sarkisyan G, Roberts AJ, Hedlund PB. The 5-HT(7) receptor as a mediator and modulator of antidepressant-like behavior. Behav Brain Res. 2010;209:99–108.
29. Mullins UL, Gianutsos G, Eison AS. Effects of antidepressants on 5-HT7 receptor regulation in the rat hypothalamus. Neuropsychopharmacology. 1999;21:352–67.
30. Sowa-Kucma M, et al. Vortioxetine: a review of the pharmacology and clinical profile of the novel antidepressant. Pharmacol Rep. 2017;69:595–601.
31. Vadodaria KC, Amatya DN, Marchetto MC, Gage FH. Modeling psychiatric disorders using patient stem cell-derived neurons: a way forward. Genome Med. 2018;10:1.
32. Rush AJ, et al. An evaluation of the quick inventory of depressive symptomatology and the hamilton rating scale for depression: a sequenced treatment alternatives to relieve depression trial report. Biol Psychiatry. 2006;59:493–501.
33. Marchetto MC, et al. Altered proliferation and networks in neural cells derived from idiopathic autistic individuals. Mol Psychiatry. 2017;22:820–35.
34. Dobin A, et al. STAR: ultrafast universal RNA-seq aligner. Bioinformatics. 2013;29:15–21.
35. Liao Y, Smyth GK, Shi W. featureCounts: an efficient general purpose program for assigning sequence reads to genomic features. Bioinformatics. 2014;30:923–30.
36. Anders S, Huber W. Differential expression analysis for sequence count data. Genome Biol. 2010;11:R106.
37. Santos R, et al. Differentiation of inflammation-responsive astrocytes from glial progenitors generated from human induced pluripotent stem cells. Stem Cell Rep. 2017;8:1757–69.